



Cite this: *Phys. Chem. Chem. Phys.*,  
2025, 27, 21544

## Embedding a guest gold cluster in an organic host. Evaluation of the encapsulation nature in a $\text{Au}_{18}$ –superphane host–guest aggregate

Margot Paco-Chipana,<sup>a</sup> Peter L. Rodríguez-Kessler<sup>b</sup> and Alvaro Muñoz-Castro   \*

Formation of supramolecular aggregates incorporating  $\text{Au}_{18}$  into a suitable bioinspired polyfunctional superphane cavity provides novel functionality to the overall structure. We evaluated the favorable incorporation of the  $\text{Au}_{18}$  cluster into the superphane cavity. This amounted to  $-145.3 \text{ kcal mol}^{-1}$ , provided mainly by electrostatic-type interactions (54.9%). Charge transfer characteristics involving host  $\leftarrow$  guest and host  $\rightarrow$  guest backdonation through  $\text{S} \leftarrow \text{Au}$  and  $\text{S} \rightarrow \text{Au}$  contacts led to overall  $\text{Au}_{18} \rightarrow \mathbf{1}$  superphane charge transfer. Charge transfer consisted of a charge hopping rate ( $k_{\text{CT}}$ ) in the range of ultrafast electron transfer, calculated to be  $2.2 \times 10^{13} \text{ s}^{-1}$  at 300 K. Thus,  $\text{Au}_{18} \rightarrow \mathbf{1}$  charge transfer was driven by coordinating and short contacts towards the superphane available cavity, resulting in a supramolecular structure of the donor–acceptor (D–A) system. We expect that the current approach can be useful for further rationalizing the relevant stabilizing factors to ensure the stable aggregation of metallic clusters in organic host cavities during the making of novel functional cluster-based host–guest aggregates.

Received 27th May 2025,  
Accepted 11th September 2025

DOI: 10.1039/d5cp01989c

rsc.li/pccp

## Introduction

A supramolecular assembly represents a useful strategy to design and achieve multifunctional aggregate materials with applications in a wide range of fields,<sup>1–6</sup> highlighting the use of non-covalent interactions in creating ordered architectures. Host–guest chemistry takes advantage of such interactions by including guest units into a suitable host cavity based on the mutual recognition between molecular constituents,<sup>7–17</sup> largely exemplified by involving organic pairs.

Recently, Zhang and coworkers reported the ferritin-inspired design,<sup>18</sup> characterizations and performance of a host–guest structure of a bare gold nanocluster (AuNC) embedded into a highly polyfunctional superphane cavity.<sup>19</sup> It involved several coordination sites given by nitrogen, oxygen and sulfur atoms from imine, BINOL (BINOL = 1,1-binaphthyl-2,2 diol) dimethyl ether,<sup>20</sup> and thiophene groups. The resulting superphane appeared as a prototypical organic cavity with multiple coordinating sites serving as guidance for further development of host structures prone to incorporate bare clusters, favoring a controlled synthesis, size-selectivity purification, solubility in

non-polar solvents, incorporation into organic electronic devices, among other issues relevant for emergent applications of atomically precise metal nanoclusters.<sup>21–33</sup>

The AuNC–superphane host–guest pair by Zhang and colleagues was obtained by reacting the hollow superphane with  $\text{AuCl}_3$  in  $\text{CH}_2\text{Cl}_2$ , followed by the addition of  $\text{NaBH}_3\text{CN}$  as a mild reducing agent,<sup>19</sup> and confirmation of the inclusion of the atomically-precise  $\text{Au}_{18}$  bare cluster *via* electrospray ionization-mass spectrometry (ESI-MS). The resulting organic–inorganic host–guest structure from AuNC–superphane gives rise to a supramolecular hybrid system that can modify the inherent physical-chemical characteristics of each constituent significantly,<sup>19</sup> as observed for different hybrid assemblies.<sup>34–41</sup> In particular, this aggregate enhances the stability of AuNCs, providing unexpected functionality as given by a broad absorption, improving the sunlight absorption capabilities, with a promising photothermal conversion efficiency of 92.8% desired for solar-to-vapor generation.<sup>19</sup>

Interestingly, the  $\text{Au}_{18}$  cluster features 18 cluster electrons (18-ce) fulfilling an electronic shell order in analogy to isolated atoms<sup>42</sup> ascribed by  $1\text{S}^2 1\text{P}^6 1\text{D}^{10}$ , in line with the superatom approach of molecular clusters providing chemical stability.<sup>43–45</sup> Theoretical calculations on the structure of the  $\text{Au}_{18}$ –superphane species<sup>19</sup> have denoted a favorable match between the available host cavity and guest size, showing coordination mainly ascribed to the thiophene and BINOL sites.

Herein, we rationalized the nature of the superphane– $\text{Au}_{18}$  interaction to further clarify the stabilizing factors that provide efficient cluster encapsulation into the available organic cavity.

<sup>a</sup> Doctorado en Biología Computacional, Facultad de Ingeniería, Universidad San Sebastián, Bellavista 7, Santiago 8420524, Chile

<sup>b</sup> Centro de Investigaciones en Óptica A.C., Loma del Bosque 115, Col. Lomas del Campestre, León, Guanajuato 37150, Mexico

<sup>c</sup> Facultad de Ingeniería, Universidad San Sebastián, Bellavista 7, Santiago 8420524, Chile. E-mail: alvaro.munoz@uss.cl

The intermolecular interaction between  $\text{Au}_{18}$  and the superphane host cavity was evaluated by energy decomposition analysis (EDA),<sup>46,47</sup> electrostatic potential maps,<sup>48–50</sup> electron density difference maps, and non-covalent index (NCI) analysis<sup>51,52</sup> to reveal the contributing role of the different constituent sections of the organic cavity. Moreover, the charge transfer of electrons was evaluated within the Marcus theory framework to account for the reorganization energy ( $\lambda$ ) and electronic coupling ( $\mathcal{V}$ ) involved in the processes determining the charge hopping rate in the resulting  $\text{Au}_{18}$ –superphane aggregate. This was done to further explore the charge transfer parameters in metallic clusters embedded in suitable organic cavities.

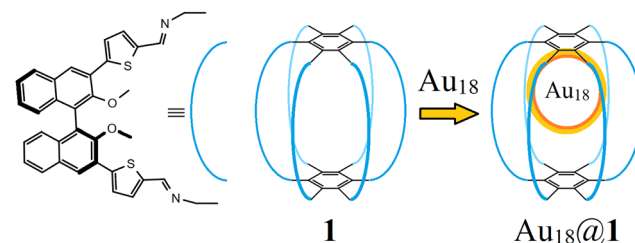
## Computational details

Calculations were done using the ADF2024 code.<sup>53</sup> We used the triple- $\zeta$  and two polarization functions (STO-TZ2P) basis set within the generalized gradient approximation (GGA) according to the BP86 exchange–correlation functional and the empirical dispersion correction to DFT (DFT-D) given by the pairwise Grimme correction (D3)<sup>54–57</sup> and Becke–Johnson damping functions.<sup>58,59</sup> Dispersion-corrected DFT methods offer reliable results and improved performance in the description of supramolecular interactions at a moderate computational cost for larger systems.<sup>55,60,61</sup> Relaxed structures were obtained through the analytical energy gradient method implemented by Versluis and Ziegler<sup>62</sup> at the TZ2P/BP86-D3 level without any symmetry restraint. The energy convergence criterion was set to  $10^{-5}$  Hartree, gradient convergence criteria to  $10^{-4}$  Hartree per Å, and radial convergence criteria to  $10^{-3}$  Å to achieve final optimized structures. The counterpoise correction scheme was employed to overcome basis set superposition error (BSSE) in the interaction energy analysis owing to the systematic error introduced by the use of finite basis sets, overbinding van der Waals aggregates.<sup>63–65</sup> Solvent effects were taken into account *via* the conductor-like screening model (COSMO) for explicit solvation using dichloromethane ( $\text{CH}_2\text{Cl}_2$ ) as the solvent, as implemented in the ADF code.<sup>66,67</sup> The charge hopping rate ( $k_{\text{CT}}$ ) in the  $\text{Au}_{18}$ –superphane aggregate was modeled using the high-temperature limit of the Marcus theory,<sup>68–72</sup> as implemented in the ADF code.

Molecular dynamics trajectories were obtained *via* eXtended tight binding (xTB) methods at the GFN0-xTB level as implemented in the standalone xtb code version.<sup>73</sup> The temperature was set to 298.15 K for thermostatistical evaluation, whereby hydrogens were treated as deuterium atoms with an accuracy set to 2.0.

## Results and discussion

The structure of  $\text{Au}_{18}$ –superphane has been provided computationally by Zhang and coworkers.<sup>19</sup> It denotes the suitable incorporation of the  $\text{Au}_{18}$  cluster into the organic host cavity. The thiophene–BINOL-based superphane host (**1**)<sup>19</sup> has been inspired by the unique binding pockets from ferritin iron storage proteins,<sup>18</sup> leading to the encapsulation and stabilization of



**Scheme 1** A schematic representation of the thiophene–BINOL-based superphane host (**1**) and its host–guest complex with  $\text{Au}_{18}$  ( $\text{Au}_{18}@\mathbf{1}$ ).

metal ions or clusters, thereby ensuring long-term stability. The resulting host–guest structure from  $\text{Au}_{18}$  and **1** involves several coordinating sites retaining the gold nanoparticle (Scheme 1). This offers an interesting case of an amenable host cavity to evaluate the role of different stabilizing contributions resulting in efficient aggregation. This approach led to the characterized  $\text{Au}_{18}@\mathbf{1}$  as probed by ESI-MS, UV-vis spectroscopy, CD spectroscopy, powder X-ray diffraction (PXRD), and X-ray photoelectron spectroscopy (XPS), among other techniques.<sup>19</sup>

Our calculations revealed a similar structure to that reported previously.<sup>19</sup> We documented shorter  $\text{Au}_{18}$  superphane bond lengths in the range 2.406–2.517 Å involving Au–S coordinating bonds from thiophene groups, and Au–O bonds in the range 2.466–3.393 Å from methyl ether groups from methylated BINOL, ascribed mainly to the upper and central sections of the organic cavity, respectively (Fig. 1c), locating the  $\text{Au}_{18}$  at one side of the available cavity. Such sections featured the main coordinating sites from the host cage interacting towards the bare  $\text{Au}_{18}$  cluster, with complementary  $\text{Au}\cdots\text{H}_3\text{C}$ - and  $\text{Au}\cdots\text{H}$ –thiophene contacts (Fig. 1d). For comparison, the central disposition of the  $\text{Au}_{18}$  cluster into **1** was evaluated, which was disfavored by 18.6 kcal mol<sup>−1</sup>.

The available cavity size in **1** was evaluated by MolvoVol suite<sup>74</sup> employing two spherical probes to define the available cavities and the related surfaces and volumes. This evaluation led to an inner cavity in **1** of  $731.84\text{ }\text{\AA}^3$  (Fig. 1d and e), which was very suitable for incorporating the  $\text{Au}_{18}$  structure with a volume of  $552.98\text{ }\text{\AA}^3$ .

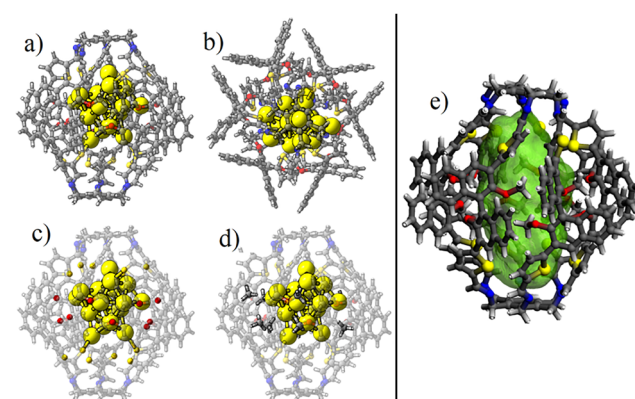


**Fig. 1** Side (a) and upper (b) views of  $\text{Au}_{18}@\mathbf{1}$ , denoting the location of methyl ether groups from methylated BINOL (c) and  $\text{Au}\cdots\text{H}_3\text{C}$ - and  $\text{Au}\cdots\text{H}$ –thiophene contacts (d). The available internal cavity size is given in green from MolvoVol suite<sup>74</sup> calculations (e).

The embedded  $\text{Au}_{18}$  cluster features 18 cluster electrons as provided by the respective set of  $6s^1$  atomic shells,<sup>44,75</sup> building up an electronic shell resembling atomic orbitals fulfilling an  $1S^21P^61D^{10}$  order, ascribed as a superatom, denoting particular stability.<sup>76–79</sup> The  $1D^{10}$  shell contributed to the formation of frontier orbitals in the overall  $\text{Au}_{18}@\mathbf{1}$  aggregate (Fig. S1, SI). This superatom cluster showed a distorted structure, which was located 34.6 kcal mol<sup>-1</sup> above the preferred isomer (Fig. S2, SI) observed from infrared multiple photon dissociation (IR-MPD) experiments.<sup>80</sup> Hence, the  $\text{Au}_{18}$  cluster could modify its structure to maximize the interaction towards the organic cavity, retaining a similar electronic structure. We wished to evaluate the interaction energy leading to the  $\text{Au}_{18}$ –superphane host–guest aggregate. Hence, the interaction between the  $\text{Au}_{18}$  unit and superphane structure **1** was calculated, resulting in a sizable stabilization of  $-145.3$  kcal mol<sup>-1</sup> (Table 1).<sup>81–83</sup> To bring host and guest units from their isolated relaxed structures to their structure in the resulting host–guest system, the involved geometric and electronic destabilizing deformation is accounted for by the preparation energy  $\Delta E_{\text{prep}}$ .<sup>81–84</sup> The estimated  $\Delta E_{\text{prep}}$  amounted to 34.6 kcal mol<sup>-1</sup> for  $\text{Au}_{18}$  and 41.8 kcal mol<sup>-1</sup> for the superphane cage, leading to an overall  $\Delta E_{\text{prep}}$  of 76.4 kcal mol<sup>-1</sup>. Hence, the structure could overcome the required structural modification to give rise to the host–guest aggregate.

The characteristics of the stabilizing host–guest interaction was further unraveled by the role of different contributing terms to the resulting interaction energy ( $\Delta E_{\text{int}}$ ) evaluated *via* the energy decomposition analysis (EDA) given by Ziegler and Rauk,<sup>46,85,86</sup> according to eqn (1):

$$\Delta E_{\text{int}} = \Delta E_{\text{Pauli}} + \Delta E_{\text{elstat}} + \Delta E_{\text{orb}} + \Delta E_{\text{disp}} \quad (1)$$

In this framework, the Pauli repulsion ( $\Delta E_{\text{Pauli}}$ ) results from the four electrons/two orbitals between occupied orbitals from  $\text{Au}_{18}$  and the superphane cavity, reflecting the steric effect associated with the interaction,<sup>87</sup> which amounted to 783.8 kcal mol<sup>-1</sup> (Table 1). Moreover, the stabilizing electronic part of the interaction involving electrostatic ( $\Delta E_{\text{elstat}}$ ) and orbital ( $\Delta E_{\text{orb}}$ ) terms accounts for the Coulomb interaction between the charge densities ( $\Delta E_{\text{elstat}}$ ) and polarization and charge transfer contribution after relaxing the orbitals ( $\Delta E_{\text{orb}}$ ) to the in the host–guest system.<sup>88</sup> The dispersion interaction ( $\Delta E_{\text{disp}}$ ) was evaluated *via* the pairwise correction of Grimme (DFT-D3).<sup>57</sup> The  $\Delta E_{\text{elstat}}$  and  $\Delta E_{\text{orb}}$  terms amounted to  $-510.4$  and  $-277.7$  kcal mol<sup>-1</sup>, respectively, complemented with the  $\Delta E_{\text{disp}}$  term of  $-140.8$  kcal mol<sup>-1</sup>, which could overcome the Pauli

**Table 1** Energy decomposition analysis for the  $\text{Au}_{18}$ –**1** interaction and for related models of **1**. Values are in kcal mol<sup>-1</sup>. Percentage contributions for stabilizing terms are provided

	$\text{Au}_{18}$ – <b>1</b>	$\text{Au}_{18}$ –( $\text{C}_4\text{H}_4\text{S}$ ) <sub>4</sub>	$\text{Au}_{18}$ –( $\text{OMe}_2$ ) <sub>12</sub>
$\Delta E_{\text{prep}}$	76.4		
$\Delta E_{\text{Pauli}}$	783.8	387.2	301.46
$\Delta E_{\text{elstat}}$	-510.4	54.9%	-263.3
$\Delta E_{\text{orb}}$	-277.7	29.9%	-153.8
$\Delta E_{\text{disp}}$	-140.8	15.2%	-24.1
$\Delta E_{\text{int}}$	-145.3		-53.9

repulsion. The percentage relationship between the stabilizing terms ( $\Delta E_{\text{orb}}$ ,  $\Delta E_{\text{elstat}}$ , and  $\Delta E_{\text{disp}}$ ) characterize the overall nature of the host–guest interaction, which was of mainly electrostatic character (54.9%), followed by an orbital contribution of 29.9% and, lastly, 15.2% from the dispersion interaction.

To reveal the spatial distribution of the main electrostatic interaction accounting for the  $\Delta E_{\text{elstat}}$  term, the charge reorganization at the van der Waals surface for  $\text{Au}_{18}$  was obtained by representing the electrostatic potential<sup>48</sup> over an electron density surface of 0.001 electrons per Bohr<sup>3</sup>.<sup>89,90</sup> The electrostatic potential for the isolated  $\text{Au}_{18}$  guest unit showed the formation of charge depletion regions as Lewis acidic sites at the low connected Au atoms (Fig. 2a) as the maxima in the surface electrostatic potential ( $V_{\text{S},\text{max}}$ ), similar to that obtained for the  $\text{Au}_{13}$  cluster,<sup>50</sup> denoted as  $\sigma$ -hole regions accounting for reactive sites in metallic clusters.<sup>50,91–93</sup> Interestingly, the electrostatic potential for the overall  $\text{Au}_{18}$ –superphane structure showed charge reorganization over the van der Waals  $\text{Au}_{18}$  surface at the Au–S and Au–O coordinating sites and also for Au···H<sub>3</sub>C- and Au···H-thiophene contacts (Fig. 2b). These data showed that the stabilizing  $\Delta E_{\text{elstat}}$  term was given by the contribution from different complementary sites within the superphane cavity contributing to encapsulation of the  $\text{Au}_{18}$  bare superatom.

Moreover,  $\Delta E_{\text{orb}}$  can be evaluated in terms of individual deformation density channels accounting for individual bonding contributions<sup>94,95</sup> *via* the natural orbitals for chemical valence<sup>96–98</sup> extension of EDA (EDA-NOCV).<sup>98</sup> We documented sixteen main individual deformation density channels ( $\Delta\rho_1$ – $\Delta\rho_{16}$ ) (Fig. S3, SI) contributing between  $-20.0$  to  $-5.2$  kcal mol<sup>-1</sup> (Table S1, SI). These data suggested host  $\leftarrow$  guest charge transfer through S  $\leftarrow$  Au contacts ( $\Delta\rho_1$ – $\Delta\rho_4$ ) (Fig. 3a), and host  $\rightarrow$  guest charge transfer *via* S  $\rightarrow$  Au contacts. These results suggested a donation and backdonation of charge leading to an overall  $\text{Au}_{18} \rightarrow \mathbf{1}$  superphane charge transfer of  $+0.79e$  as obtained from Hirshfeld charge analyses. The spatial distribution of the resulting charge transfer was denoted by the difference in electron density between the host–guest aggregate and respective fragments ( $\Delta\rho(r) = \rho(r)^{\text{total}} - (\rho(r)^{\text{Au}_{18}} + \rho(r)^{\text{superphane}})$ ) (Fig. 3b). These data suggested that charge accumulation remained at the host cavity near the  $\text{Au}_{18}$  cluster, with charge depletion at the S–Au coordinating contacts. Thus, the

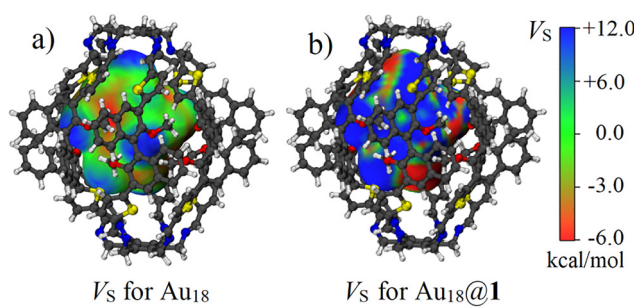


**Fig. 2** The electrostatic potential surface for the isolated  $\text{Au}_{18}$  cluster (a) and overall  $\text{Au}_{18}@\mathbf{1}$  (b) aggregate drawn at a 0.001 electrons per Bohr<sup>3</sup> electron density for the  $\text{Au}_{18}$  cluster (including the **1** host structure for graphical guidance). Blue denotes electro-positive sites prone to interact with Lewis bases.

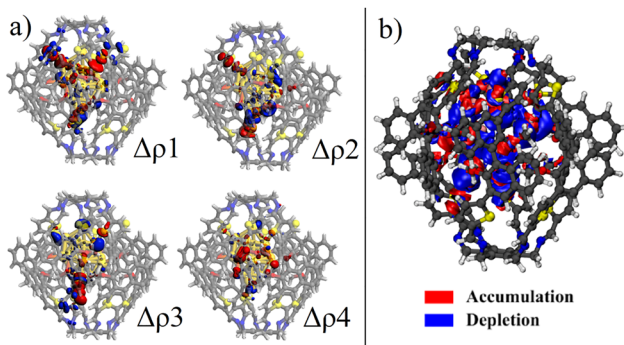


Fig. 3 Side (a) and upper (b) views of  $\text{Au}_{18}@\mathbf{1}$ , denoting the location of methyl ether groups from methylated BINOL (c) and  $\text{Au}\cdots\text{H}_3\text{C}$ - and  $\text{Au}\cdots\text{H}-\text{thiophene}$  contacts.

$\text{Au}_{18} \rightarrow \mathbf{1}$  charge transfer was driven by coordinating and short contacts towards the superphane available cavity, resulting in a supramolecular donor-acceptor (D-A) system structure. In addition, TZ2P/PBE-D3 and TZ2P/B3LYP-D3 levels of theory were evaluated, which delivered similar features than for those calculated at the TZ2P/BP86-D3 level, supporting the calculated data at different computational levels (Table S2, SI). The obtained  $\text{Au}_{18}\cdots\mathbf{1}$  interaction energy amounted to  $-133.6$  and  $-155.5$  kcal mol $^{-1}$  for TZ2P/PBE-D3 and TZ2P/B3LYP-D3 levels, respectively, in line with that calculated at TZ2P/BP86-D3 ( $-145.2$  kcal mol $^{-1}$ ). In addition, different levels of theory can be employed to gain insights into the characteristics of the  $\text{Au}_{18}$  inclusion into  $\mathbf{1}$ .<sup>99</sup>

Furthermore, the contribution of London interactions as complementary weak intermolecular interactions for the overall host-guest aggregation were evaluated in the interacting structure *via* the independent gradient model (IGM).<sup>100-102</sup> This approach enabled isolation of the intermolecular interaction between the host and guest *via* the proposed electron-density based  $\delta g_{\text{inter}}$  descriptor by Hénon<sup>102</sup> and coworkers. The stabilizing and repulsive characteristics of the intermolecular interaction can be evaluated by the second eigenvalue of the electron density Hessian ( $\lambda_2$ ). This accounts for an accumulation (attractive) or depletion (repulsive) of electron density, with the  $\text{sign}(\lambda_2)\rho$  term as a useful descriptor for stabilizing ( $\lambda_2 < 0$ ), van der Waals ( $\lambda_2 \approx 0$ ) or repulsive-type interactions ( $\lambda_2 > 0$ ).<sup>51,52,103</sup> IGM analysis was carried out as implemented in the Multiwfn suite.<sup>104</sup>

The resulting intermolecular interactions from the IGM analysis (Fig. 4) were mainly ascribed at S-Au contact sites, regions below the methyl ether units from BINOL motifs given as  $\text{Au}\cdots\text{OMe}$  and  $\text{Au}\cdots\text{H}_3\text{C}$ -, and  $\text{Au}\cdots\text{H}-\text{thiophene}$  contacts. These results suggested that non-covalent contributions to the  $\text{Au}_{18}$  encapsulation interactions were due to the multiple interacting sites from the organic cavity.

Moreover, a simplified model involving the four closest thiophene groups retaining their structure in the overall host-guest aggregate ( $\text{Au}_{18}@\text{(SC}_4\text{H}_4)_4$ ) was used to evaluate the contribution of units from  $\text{Au-S}$  and  $\text{Au}\cdots\text{H}-\text{thiophene}$  contacts (Fig. S4, SI). This model revealed an interaction energy of  $-53.9$  kcal mol $^{-1}$ , which accounted for 37.1% from the

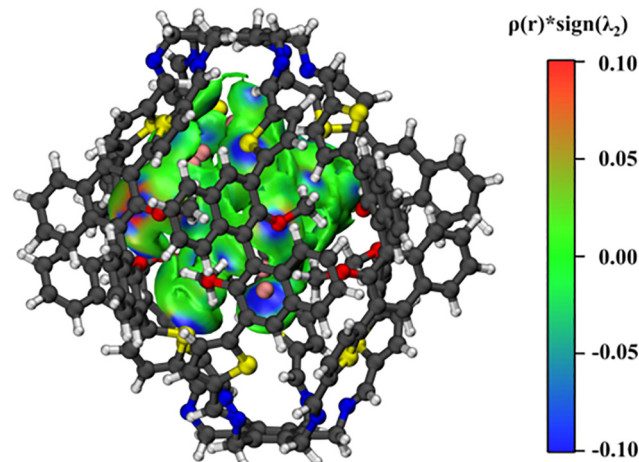


Fig. 4 The independent gradient model (IGM) isosurface (0.005 a.u.), colored in the  $-0.10$  a.u.  $< \text{sign}(\lambda_2)\rho < +0.10$  a.u. range for the  $\text{Au}_{18}\cdots\mathbf{1}$  interaction in  $\text{Au}_{18}@\mathbf{1}$ . Blue/red accounts for stabilizing/destabilizing non-covalent interactions, whereas green isosurfaces denote London-type interactions.

overall  $\text{Au}_{18}\cdots\mathbf{1}$  interaction energy in the  $\text{Au}_{18}@\mathbf{1}$  aggregate. Similarly, for the simplified model accounting for  $\text{Au}\cdots\text{OMe}$  and  $\text{Au}\cdots\text{H}_3\text{C}$ - interactions ( $\text{Au}_{18}@\text{(OMe}_2)_4$ ), the interaction energy towards the  $\text{Au}_{18}$  cluster amounted to  $-59.7$  kcal mol $^{-1}$ , representing 41.1% from the overall interaction energy related to the encapsulation of  $\text{Au}_{18}$  into  $\mathbf{1}$  superphane. The remaining contribution to the overall interaction energy related to formation of the  $\text{Au}_{18}@\mathbf{1}$  aggregate was given by weaker contributions from several  $\text{Au}_{18}\cdots\text{HC}\equiv\text{N}$ - contacts at one side of the cavity. Hence, efficient encapsulation of the  $\text{Au}_{18}$  cluster was provided by the contribution of several weak interactions driven by the contacts to the superphane cavity.

Furthermore, the resulting incorporation of  $\text{Au}_{18}$  can involve complex and diverse conformational landscapes.<sup>105,106</sup> Conformational exploration was evaluated through molecular dynamics *via* eXtended tight binding (xTB) methods at the GFN0-xTB level within the xtb code.<sup>73</sup> The resulting trajectory involved structures with a more disperse  $\text{Au}_{18}$  cluster within the  $\mathbf{1}$  cage (red arrow in Fig. 5), a partially aggregated  $\text{Au}_{18}$  structure (blue arrow), and a completely aggregated  $\text{Au}_{18}$  as the most favorable structure (green arrow). Along with the trajectory steps, different Au-cage interactions evolve whereby  $\text{Au}_{18}$  tends to aggregate as characterized previously.<sup>19</sup> Recently, a benchmark report on the capabilities of xTB Hamiltonians (GFN0-xTB, GFN1-xTB, and GFN2-xTB) in achieving host-guest binding features with implicit solvent models<sup>107</sup> denoted their performance in relation to MM-based techniques, appearing to be worthy alternatives if MM-based techniques are not applicable. In our case, due to the hybrid metallic-organic nature of the  $\text{Au}_{18}$ -superphane aggregate, only GFN0-xTB could be applied successfully, and the resulting trajectory should be regarded as a qualitative conformational sampling, whereby quantitative interaction energy analyses were reliant upon DFT calculations.

The initial and middle stages of the calculated molecular dynamics trajectory in Fig. 5 are shown by red and blue arrows,

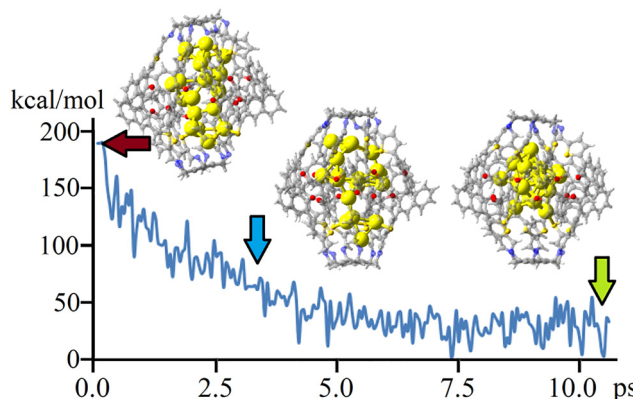


Fig. 5 Molecular dynamic trajectories for the  $\text{Au}_{18}@\mathbf{1}$  structure featuring a disperse  $\text{Au}_{18}$  cluster isomer (red arrow), a partially aggregated  $\text{Au}_{18}$  structure (blue arrow), and a complete aggregated  $\text{Au}_{18}$  structure (green arrow). The x-axis corresponds to 200 steps, covering a total simulation time of 10 ps.

respectively. The calculated  $\text{Au}_{18}$ -superphane interaction energy at these stages (Table S3) showed a repulsive interaction of  $+82.6 \text{ kcal mol}^{-1}$  at the initial step, which stabilized to  $-35.2 \text{ kcal mol}^{-1}$  at the middle position of the trajectory, and settled at the interaction value of  $-145.2 \text{ kcal mol}^{-1}$  for the  $\text{Au}_{18}@\mathbf{1}$  structure discussed above. The main destabilizing factor was provided by an increase in the Pauli repulsion contribution at initial and middle steps. Hence, the more compact  $\text{Au}_{18}$  structure (final), as discussed above, provided more favorable encapsulation reducing the steric repulsion towards the overall cavity, in contrast to when more gold atoms are spread around the cavity. Thus, the compact metal cluster distribution favored a reduction in the steric repulsion upon encapsulation, thereby leading to more stable cluster incorporation.

We wished to evaluate the intermolecular charge transfer characteristics in the formation of  $\text{Au}_{18}@\mathbf{1}$ . Hence, the electronic coupling between  $\text{Au}_{18}$  and superphane host was calculated to quantify charge transport capabilities. Calculations revealed strong electronic coupling of 52.1 meV for electron transport ( $V_e$ ) and 45.8 meV for hole transport ( $V_h$ ) integrals. These values are in the range of one of the most efficient p-type semiconductors: benzothienobenzothiophene (BTBT) (33 meV for hole transport).<sup>108</sup> The charge hopping rate ( $k_{\text{CT}}$ ) in  $\text{Au}_{18}@\mathbf{1}$  can be modeled using the high-temperature limit of the Marcus theory.<sup>68–72</sup> The latter is governed by two key parameters, the reorganization energy ( $\lambda$ ) and intermolecular effective electronic coupling for electron transport ( $V$ ),<sup>68–72</sup> where  $T$  is the temperature and  $k_b$  is the Boltzmann constant, as given by eqn (2):

$$k_{\text{CT}} = \frac{V^2}{\hbar} \sqrt{\frac{\pi}{\lambda k_b T}} \exp\left(-\frac{\lambda}{4k_b T}\right) \quad (2)$$

The adiabatic potential energy surfaces method was used to calculate the reorganization energy ( $\lambda$ ).<sup>109</sup> This involved the neutral and anionic optimized geometries of the isolated guest and host at neutral and anionic states, given by  ${}^G E_0$  and  ${}^G E_-$ , and  ${}^H E_0$  and  ${}^H E_-$ , respectively, taking into account solvation

effects *via* the COSMO approach amounting to 0.17 eV, which is given by eqn (3):

$$\begin{aligned} \lambda = \lambda_0 + \lambda_- = & ({}^H E_0^{\text{anion}} - {}^H E_0^{\text{neutral}} + {}^G E_0^{\text{anion}} - {}^G E_0^{\text{neutral}}) \\ & + ({}^H E_-^{\text{neutral}} - {}^H E_-^{\text{anion}} + {}^G E_-^{\text{neutral}} - {}^G E_-^{\text{anion}}) \end{aligned} \quad (3)$$

As a result, the estimated intermolecular charge hopping rate ( $k_{\text{CT}}$ ) was  $2.2 \times 10^{13} \text{ s}^{-1}$  at 300 K, in the range of ultrafast electron transfer in supramolecular aggregates ( $4.0 \times 10^{11} \text{ s}^{-1}$ ),<sup>110</sup> and from other intermolecular interactions ( $5.0 \times 10^{12} \text{ s}^{-1}$ ).<sup>111</sup> Thus, the  $\text{Au}_{18} \rightarrow \mathbf{1}$  charge transfer was driven by coordinating and short contacts towards the superphane available cavity, resulting in a supramolecular structure of donor( $\text{Au}_{18}$ )-acceptor(superphane) D-A system.

## Conclusions

The favorable incorporation of the  $\text{Au}_{18}$  cluster into the poly-functional superphane cavity **1** amounted to  $-145.3 \text{ kcal mol}^{-1}$ , mainly provided by electrostatic-type interactions (54.9%), leading to a stable  $\text{Au}_{18}@\mathbf{1}$  aggregate. The electrostatic contribution was given by charge reorganization over  $\text{Au}_{18}$ , which enhanced the interaction towards the **1** cavity, and accounted for the observed stability of the overall host-guest pair. Charge transfer involved host  $\leftarrow$  guest and host  $\rightarrow$  guest backdonation through S  $\leftarrow$  Au and S  $\rightarrow$  Au contacts, leading to an overall  $\text{Au}_{18} \rightarrow \mathbf{1}$  superphane charge transfer of  $+0.79e$ . Hypothetical models involving isolated cavity units suggested that the  $\text{Au}_{18}$ -thiophane interaction amounted to  $-53.9 \text{ kcal mol}^{-1}$ , accounting for 37.1% of the overall stabilization, whereas the isolated methyl ether units from BINOL motifs amounted to  $-59.7 \text{ kcal mol}^{-1}$ , accounting for 41.1% of the  $\text{Au}_{18}@\mathbf{1}$  aggregate stabilization. Moreover, non-covalent interactions contributed to a lesser extent to  $\text{Au}_{18}@\mathbf{1}$  formation.

The resulting aggregate showed favorable charge transfer. A charge hopping rate ( $k_{\text{CT}}$ ) in the range of ultrafast electron transfer, calculated to be  $2.2 \times 10^{13} \text{ s}^{-1}$  at 300 K, was documented. Thus, the  $\text{Au}_{18} \rightarrow \mathbf{1}$  charge transfer was driven by coordinating and short contacts towards the superphane available cavity, resulting in the supramolecular structure of the D-A system.

We expect that the current approach could help to characterize further the stabilizing factors leading to the aggregation of metallic clusters into organic host cavities. This strategy may aid rational design and explorative synthetic efforts, providing novel functionality for host-guest aggregates.

## Conflicts of interest

There are no conflicts of interest to declare.

## Data availability

The data supporting this article have been included as part of the supplementary information (SI). Supplementary information is available. See DOI: <https://doi.org/10.1039/d5cp01989c>.

## Acknowledgements

M. P.-C. acknowledges a PhD scholarship from Vicerrectoría de Investigación y Doctorados, Universidad San Sebastián. This work was supported by ANID FONDECYT Regular 1221676. P. L. R.-K. would like to thank the CIMAT Supercomputing Laboratories of Guanajuato and Puerto Interior for their support.

## References

- 1 G. T. Williams, C. J. E. Haynes, M. Fares, C. Caltagirone, J. R. Hiscock and P. A. Gale, Advances in applied supramolecular technologies, *Chem. Soc. Rev.*, 2021, **50**, 2737–2763.
- 2 F. Huang and E. V. Anslyn, Introduction: Supramolecular Chemistry, *Chem. Rev.*, 2015, **115**, 6999–7000.
- 3 P. Commins, M. B. Al-Handawi and P. Naumov, Self-healing crystals, *Nat. Rev. Chem.*, 2025, **9**, 343–355.
- 4 W. He, Y. Yu, K. Iizuka, H. Takezawa and M. Fujita, Supramolecular coordination cages as crystalline sponges through a symmetry mismatch strategy, *Nat. Chem.*, 2025, **17**, 653–662.
- 5 H.-N. Zhang and G.-X. Jin, Synthesis of molecular Borromean links featuring trimeric metallocages, *Nat. Synth.*, 2025, **4**, 488–496.
- 6 C. Li, A. Iscen, H. Sai, K. Sato, N. A. Sather, S. M. Chin, Z. Álvarez, L. C. Palmer, G. C. Schatz and S. I. Stupp, Supramolecular-covalent hybrid polymers for light-activated mechanical actuation, *Nat. Mater.*, 2020, **19**, 900–909.
- 7 D. Zhang, A. Martinez and J.-P. Dutasta, Emergence of Hemicryptophanes: From Synthesis to Applications for Recognition, Molecular Machines, and Supramolecular Catalysis, *Chem. Rev.*, 2017, **117**, 4900–4942.
- 8 D. Prochowicz, A. Kornowicz and J. Lewiński, Interactions of Native Cyclodextrins with Metal Ions and Inorganic Nanoparticles: Fertile Landscape for Chemistry and Materials Science, *Chem. Rev.*, 2017, **117**, 13461–13501.
- 9 G. Yu, K. Jie and F. Huang, Supramolecular Amphiphiles Based on Host–Guest Molecular Recognition Motifs, *Chem. Rev.*, 2015, **115**, 7240–7303.
- 10 D.-H. Qu, Q.-C. Wang, Q.-W. Zhang, X. Ma and H. Tian, Photoresponsive Host–Guest Functional Systems, *Chem. Rev.*, 2015, **115**, 7543–7588.
- 11 H. Amouri, C. Desmarests and J. Moussa, Confined Nanospaces in Metallocages: Guest Molecules, Weakly Encapsulated Anions, and Catalyst Sequestration, *Chem. Rev.*, 2012, **112**, 2015–2041.
- 12 R. D. Mukhopadhyay, G. Das and A. Ajayaghosh, Stepwise control of host–guest interaction using a coordination polymer gel, *Nat. Commun.*, 2018, **9**, 1987.
- 13 M. Zhang, Z. Gong, W. Yang, L. Jin, S. Liu, S. Chang and F. Liang, Regulating Host–Guest Interactions between Cucurbit[7]uril and Guests on Gold Surfaces for Rational Engineering of Gold Nanoparticles, *ACS Appl. Nano Mater.*, 2020, **3**, 4283–4291.
- 14 G. Kali, S. Haddadzadegan and A. Bernkop-Schnürch, Cyclodextrins and derivatives in drug delivery: New developments, relevant clinical trials, and advanced products, *Carbohydr. Polym.*, 2024, **324**, 121500.
- 15 H. Asghar, S. Bilal, M. H. Nawaz, G. Rasool and A. Hayat, Host–Guest Mechanism via Induced Fit Fullerene Complexation in Porphin Receptor to Probe Salivary Alpha-Amylase in Dental Caries for Clinical Applications, *ACS Appl. Bio Mater.*, 2024, **7**, 1250–1259.
- 16 M. Li, Y.-Q. Shi, X. Gan, L. Su, J. Liang, H. Wu, Y. You, M. Che, P. Su, T. Wu, Z. Zhang, W. Zhang, L.-Y. Yao, P. Wang and T.-Z. Xie, Coordination-Driven Tetragonal Prismatic Cage and the Investigation on Host–Guest Complexation, *Inorg. Chem.*, 2023, **62**, 4393–4398.
- 17 A. A. Ivanov, P. A. Abramov, M. Haouas, Y. Molard, S. Cordier, C. Falaise, E. Cadot and M. A. Shestopalov, Supramolecular Host–Guest Assemblies of  $[M_6Cl_{14}]^{2-}$ , M = Mo, W, Clusters with  $\gamma$ -Cyclodextrin for the Development of CLUSPOMs, *Inorganics*, 2023, **11**, 77.
- 18 N. Song, J. Zhang, J. Zhai, J. Hong, C. Yuan and M. Liang, Ferritin: A Multifunctional Nanoplatform for Biological Detection, Imaging Diagnosis, and Drug Delivery, *Acc. Chem. Res.*, 2021, **54**, 3313–3325.
- 19 Y. Zhang, J. Zhou, K. Luo, W. Zhou, F. Wang, J. Li and Q. He, Ferritin-Inspired Encapsulation and Stabilization of Gold Nanoclusters for High-Performance Photothermal Conversion, *Angew. Chem., Int. Ed.*, 2025, **64**, e202500058.
- 20 Y. Yu, Y. Hu, C. Ning, W. Shi, A. Yang, Y. Zhao, Z. Cao, Y. Xu and P. Du, BINOL-Based Chiral Macrocycles and Cages, *Angew. Chem., Int. Ed.*, 2024, **63**, e202407034.
- 21 S. Maity, S. Kolay, S. Chakraborty, A. Devi, Rashi and A. Patra, A comprehensive review of atomically precise metal nanoclusters with emergent photophysical properties towards diverse applications, *Chem. Soc. Rev.*, 2025, **54**, 1785–1844.
- 22 J. Qian, Z. Yang, J. Lyu, Q. Yao and J. Xie, Molecular Interactions in Atomically Precise Metal Nanoclusters, *Precis. Chem.*, 2024, **2**, 495–517.
- 23 R. J. Wilson, N. Lichtenberger, B. Weinert and S. Dehnen, Intermetalloid and Heterometallic Clusters Combining p-Block (Semi)Metals with d- or f-Block Metals, *Chem. Rev.*, 2019, **119**, 8506–8554.
- 24 B. Peters, N. Lichtenberger, E. Dornseipen and S. Dehnen, Current advances in tin cluster chemistry, *Chem. Sci.*, 2020, **11**, 16–26.
- 25 F. Li, A. Muñoz-Castro and S. C. S. C. Sevov,  $[Ge_9\{Si(SiMe_3)_3\}_3\{SnPh_3\}]$ : A Tetrasubstituted and Neutral Deltahedral Nine-Atom Cluster, *Angew. Chem., Int. Ed.*, 2012, **51**, 8581–8584.
- 26 A. Jana, A. R. Kini and T. Pradeep, Atomically Precise Clusters: Chemical Evolution of Molecular Matter at the Nanoscale, *AsiaChem Mag.*, 2023, **3**, 56–65.
- 27 L. He, T. Dong, D. Jiang and Q. Zhang, Recent progress in atomically precise metal nanoclusters: From bio-related properties to biological applications, *Coord. Chem. Rev.*, 2025, **535**, 216633.
- 28 J. Zhang, Z. Li, K. Zheng and G. Li, Synthesis and characterization of size-controlled atomically precise gold clusters, *Phys. Sci. Rev.*, 2018, **3**, 20170083.

29 S. Biswas, S. Das and Y. Negishi, Progress and prospects in the design of functional atomically-precise Ag(I)-thiolate nanoclusters and their assembly approaches, *Coord. Chem. Rev.*, 2023, **492**, 215255.

30 R. Nakatani, S. Das and Y. Negishi, The structure and application portfolio of intricately architected silver cluster-assembled materials, *Nanoscale*, 2024, **16**, 9642–9658.

31 T. Kawasaki, T. Okada, D. Hirayama and Y. Negishi, Atomically precise metal nanoclusters as catalysts for electrocatalytic CO<sub>2</sub> reduction, *Green Chem.*, 2024, **26**, 122–163.

32 E. Khatun and T. Pradeep, New Routes for Multicomponent Atomically Precise Metal Nanoclusters, *ACS Omega*, 2021, **6**, 1–16.

33 Y. Du, H. Sheng, D. Astruc and M. Zhu, Atomically Precise Noble Metal Nanoclusters as Efficient Catalysts: A Bridge between Structure and Properties, *Chem. Rev.*, 2020, **120**, 526–622.

34 M. A. Moussawi, N. Leclerc-Laronze, S. Floquet, P. A. Abramov, M. N. Sokolov, S. Cordier, A. Ponchel, E. Monflier, H. Bricout, D. Landy, M. Haouas, J. Marrot and E. Cadot, Polyoxometalate, Cationic Cluster, and  $\gamma$ -Cyclodextrin: From Primary Interactions to Supramolecular Hybrid Materials, *J. Am. Chem. Soc.*, 2017, **139**, 12793–12803.

35 A. A. Ivanov, C. Falaise, K. Laouer, F. Hache, P. Changenet, Y. V. Mironov, D. Landy, Y. Molard, S. Cordier, M. A. Shestopalov, M. Haouas and E. Cadot, Size-Exclusion Mechanism Driving Host–Guest Interactions between Octahedral Rhenium Clusters and Cyclodextrins, *Inorg. Chem.*, 2019, **58**, 13184–13194.

36 A. A. Ivanov, C. Falaise, A. A. Shmakova, N. Leclerc, S. Cordier, Y. Molard, Y. V. Mironov, M. A. Shestopalov, P. A. Abramov, M. N. Sokolov, M. Haouas and E. Cadot, Cyclodextrin-Assisted Hierarchical Aggregation of Dawson-type Polyoxometalate in the Presence of {Re<sub>6</sub>Se<sub>8</sub>} Based Clusters, *Inorg. Chem.*, 2020, **59**, 11396–11406.

37 A. A. Ivanov, C. Falaise, P. A. Abramov, M. A. Shestopalov, K. Kirakci, K. Lang, M. A. Moussawi, M. N. Sokolov, N. G. Naumov, S. Floquet, D. Landy, M. Haouas, K. A. Brylev, Y. V. Mironov, Y. Molard, S. Cordier and E. Cadot, Host–Guest Binding Hierarchy within Redox- and Luminescence-Responsive Supramolecular Self-Assembly Based on Chalcogenide Clusters and  $\gamma$ -Cyclodextrin, *Chem. – Eur. J.*, 2018, **24**, 13467–13478.

38 H. Zhu, J. Li, J. Wang and E. Wang, Lighting Up the Gold Nanoclusters via Host–Guest Recognition for High-Efficiency Antibacterial Performance and Imaging, *ACS Appl. Mater. Interfaces*, 2019, **11**, 36831–36838.

39 S. Hu, H. Zhao, P. Xie, X. Zhu, L. Liu, N. Yin, Z. Tang, K. Peng and R. Yuan, High-efficiency electrochemiluminescence of host-guest ligand-assembled gold nanoclusters preoxidized for ultrasensitive biosensing of protein, *Sens. Actuators, B*, 2024, **419**, 136347.

40 K. I. Assaf, A. Hennig, S. Peng, D.-S. Guo, D. Gabel and W. M. Nau, Hierarchical host–guest assemblies formed on dodecaborate-coated gold nanoparticles, *Chem. Commun.*, 2017, **53**, 4616–4619.

41 K. Sahoo, T. R. Gazi, S. Roy and I. Chakraborty, Nanohybrids of atomically precise metal nanoclusters, *Commun. Chem.*, 2023, **6**, 157.

42 P. Pyykkö, Understanding the eighteen-electron rule, *J. Organomet. Chem.*, 2006, **691**, 4336–4340.

43 H. Häkkinen, in *Protected Metal Clusters: From Fundamentals to Applications*, ed. H. Häkkinen and T. Tsukuda, Elsevier Science, 2015, pp. 189–222.

44 H. Häkkinen, Atomic and electronic structure of gold clusters: understanding flakes, cages and superatoms from simple concepts, *Chem. Soc. Rev.*, 2008, **37**, 1847–1859.

45 J. U. Reveles, S. N. Khanna, P. J. Roach and A. W. Castleman, Multiple valence superatoms, *Proc. Natl. Acad. Sci. U. S. A.*, 2006, **103**, 18405–18410.

46 M. von Hopffgarten and G. Frenking, Energy decomposition analysis, *Wiley Interdiscip. Rev.: Comput. Mol. Sci.*, 2012, **2**, 43–62.

47 M. von Hopffgarten and G. Frenking, Building a bridge between coordination compounds and clusters: bonding analysis of the icosahedral molecules [M(ER)<sub>12</sub>] (M = Cr, Mo, W; E = Zn, Cd, Hg), *J. Phys. Chem. A*, 2011, **115**, 12758–12768.

48 T. Brinck, in *Theoretical and Computational Chemistry*, ed. C. Páráknyi, 1998, pp. 51–93.

49 J. Halldin Stenlid, A. J. Johansson and T. Brinck,  $\sigma$ -Holes and  $\sigma$ -lumps direct the Lewis basic and acidic interactions of noble metal nanoparticles: introducing regium bonds, *Phys. Chem. Chem. Phys.*, 2018, **20**, 2676–2692.

50 J. H. Stenlid and T. Brinck, Extending the  $\sigma$ -Hole Concept to Metals: An Electrostatic Interpretation of the Effects of Nanostructure in Gold and Platinum Catalysis, *J. Am. Chem. Soc.*, 2017, **139**, 11012–11015.

51 G. Saleh, C. Gatti and L. Lo Presti, Non-covalent interaction via the reduced density gradient: Independent atom model vs experimental multipolar electron densities, *Comput. Theor. Chem.*, 2012, **998**, 148–163.

52 G. Saleh, C. Gatti, L. Lo Presti and J. Contreras-García, Revealing Non-covalent Interactions in Molecular Crystals through Their Experimental Electron Densities, *Chem. – Eur. J.*, 2012, **18**, 15523–15536.

53 Amsterdam Density Functional (ADF 2024) Code, Vrije Universiteit: Amsterdam, The Netherlands. Available at: <https://www.scm.com>.

54 S. Grimme, Accurate description of van der Waals complexes by density functional theory including empirical corrections, *J. Comput. Chem.*, 2004, **25**, 1463–1473.

55 S. Grimme, Semiempirical GGA-type density functional constructed with a long-range dispersion correction, *J. Comput. Chem.*, 2006, **27**, 1787–1799.

56 S. Grimme, J. Antony, S. Ehrlich and H. Krieg, A consistent and accurate ab initio parametrization of density functional dispersion correction (DFT-D) for the 94 elements H–Pu, *J. Chem. Phys.*, 2010, **132**, 154104.

57 S. Grimme, Density functional theory with London dispersion corrections, *Wiley Interdiscip. Rev.: Comput. Mol. Sci.*, 2011, **1**, 211–228.

58 E. R. Johnson and A. D. Becke, A post-Hartree-Fock model of intermolecular interactions, *J. Chem. Phys.*, 2005, **123**, 024101.

59 S. Grimme, S. Ehrlich and L. Goerigk, Effect of the damping function in dispersion corrected density functional theory, *J. Comput. Chem.*, 2011, **32**, 1456–1465.

60 A. Suvitha and N. S. Venkataraman, Trapping of organophosphorus chemical nerve agents by pillar[5]arene: A DFT, AIM, NCI and EDA analysis, *J. Inclusion Phenom. Macrocyclic Chem.*, 2017, **87**, 207–218.

61 J. C. Babón, M. A. Esteruelas, I. Fernández, A. M. López and E. Oñate, Evidence for a Bis(Elongated  $\sigma$ )-Dihydrideborate Coordinated to Osmium, *Inorg. Chem.*, 2018, **57**, 4482–4491.

62 L. Versluis and T. Ziegler, The determination of molecular structures by density functional theory. The evaluation of analytical energy gradients by numerical integration, *J. Chem. Phys.*, 1988, **88**, 322–328.

63 S. Simon, M. Duran and J. J. Dannenberg, How does basis set superposition error change the potential surfaces for hydrogen-bonded dimers?, *J. Chem. Phys.*, 1996, **105**, 11024–11031.

64 F. Jensen, Basis Set Superposition Errors Are Partly Basis Set Imbalances, *J. Chem. Theory Comput.*, 2024, **20**, 767–774.

65 S. F. Boys and F. Bernardi, The calculation of small molecular interactions by the differences of separate total energies. Some procedures with reduced errors, *Mol. Phys.*, 1970, **19**, 553–566.

66 A. Klamt and V. Jonas, Treatment of the outlying charge in continuum solvation models, *J. Chem. Phys.*, 1996, **105**, 9972.

67 G. Te Velde, F. M. Bickelhaupt, E. J. Baerends, C. Fonseca Guerra, S. J. van Gisbergen, J. G. Snijders and T. Ziegler, Chemistry with ADF, *J. Comput. Chem.*, 2001, **22**, 931–967.

68 K. Senthilkumar, F. C. Grozema, F. M. Bickelhaupt and L. D. A. Siebbeles, Charge transport in columnar stacked triphenylenes: Effects of conformational fluctuations on charge transfer integrals and site energies, *J. Chem. Phys.*, 2003, **119**, 9809–9817.

69 K. Senthilkumar, F. C. Grozema, C. F. Guerra, F. M. Bickelhaupt, F. D. Lewis, Y. A. Berlin, M. A. Ratner and L. D. A. Siebbeles, Absolute Rates of Hole Transfer in DNA, *J. Am. Chem. Soc.*, 2005, **127**, 14894–14903.

70 R. A. Marcus, Electron transfer reactions in chemistry. Theory and experiment, *Rev. Mod. Phys.*, 1993, **65**, 599–610.

71 R. A. Marcus, On the Theory of Oxidation-Reduction Reactions Involving Electron Transfer. III. Applications to Data on the Rates of Organic Redox Reactions, *J. Chem. Phys.*, 1957, **26**, 872–877.

72 N. S. Hush, Adiabatic Rate Processes at Electrodes. I. Energy-Charge Relationships, *J. Chem. Phys.*, 1958, **28**, 962–972.

73 C. Bannwarth, E. Caldeweyher, S. Ehlert, A. Hansen, P. Pracht, J. Seibert, S. Spicher and S. Grimme, Extended tight-binding quantum chemistry methods, *Wiley Interdiscip. Rev.: Comput. Mol. Sci.*, 2021, **11**, e1493.

74 J. B. Maglic and R. Lavendomme, MoloVol: an easy-to-use program for analyzing cavities, volumes and surface areas of chemical structures, *J. Appl. Crystallogr.*, 2022, **55**, 1033–1044.

75 H. Häkkinen, M. Walter and H. Grönbeck, Divide and Protect: Capping Gold Nanoclusters with Molecular Gold-Thiolate Rings, *J. Phys. Chem. B*, 2006, **110**, 9927–9931.

76 D. E. Bergeron, A. W. Castleman, T. Morisato and S. N. Khanna, Formation of  $\text{Al}_{13}\text{I}$ : Evidence for the superhalogen character of  $\text{Al}_{13}$ , *Science*, 2004, **304**, 84–87.

77 A. C. Reber, S. N. Khanna and A. W. Castleman, Superatom Compounds, Clusters, and Assemblies: Ultra Alkali Motifs and Architectures, *J. Am. Chem. Soc.*, 2007, **129**, 10189–10194.

78 A. C. Reber and S. N. Khanna, Superatoms: Electronic and Geometric Effects on Reactivity, *Acc. Chem. Res.*, 2017, **50**, 255–263.

79 T. Tsukuda and H. Häkkinen, *Protected Metal Clusters: From Fundamentals to Applications*, Elsevier, 2015.

80 P. V. Nhat, N. T. Si, A. Fielicke, V. G. Kiselev and M. T. Nguyen, A new look at the structure of the neutral  $\text{Au}_{18}$  cluster: hollow versus filled golden cage, *Phys. Chem. Chem. Phys.*, 2023, **25**, 9036–9042.

81 T. Ziegler and A. Rauk, A theoretical study of the ethylene-metal bond in complexes between copper(1+), silver(1+), gold(1+), platinum(0) or platinum(2+) and ethylene, based on the Hartree-Fock-Slater transition-state method, *Inorg. Chem.*, 1979, **18**, 1558–1565.

82 M. von Hopffgarten, G. Frenking, M. von Hopffgarten and G. Frenking, Energy decomposition analysis, *Wiley Interdiscip. Rev.: Comput. Mol. Sci.*, 2012, **2**, 43–62.

83 L. Zhao, M. von Hopffgarten, D. M. Andrada and G. Frenking, Energy decomposition analysis, *Wiley Interdiscip. Rev.: Comput. Mol. Sci.*, 2018, **8**, e1345.

84 F. Kreuter and R. Tonner-Zech, Energy decomposition analysis for excited states: an extension based on TDDFT, *Phys. Chem. Chem. Phys.*, 2025, **27**, 4728–4745.

85 K. Morokuma, Molecular Orbital Studies of Hydrogen Bonds. III.  $\text{C}=\text{O}\cdots\text{H}-\text{O}$  Hydrogen Bond in  $\text{H}_2\text{CO}\cdots\text{H}_2\text{O}$  and  $\text{H}_2\text{CO}\cdots 2\text{H}_2\text{O}$ , *J. Chem. Phys.*, 1971, **55**, 1236–1244.

86 T. Ziegler and A. Rauk, Calculation of Bonding Energies by Hartree-Fock Slater Method. 1. Transition-State Method, *Theor. Chim. Acta*, 1977, **46**, 1–10.

87 B. Pinter, T. Fievez, F. M. Bickelhaupt, P. Geerlings and F. De Proft, On the origin of the steric effect, *Phys. Chem. Chem. Phys.*, 2012, **14**, 9846.

88 P. Su and H. Li, Energy decomposition analysis of covalent bonds and intermolecular interactions, *J. Chem. Phys.*, 2009, **131**, 014102.

89 F. A. Bulat, A. Toro-Labbé, T. Brinck, J. S. Murray and P. Politzer, Quantitative analysis of molecular surfaces: areas, volumes, electrostatic potentials and average local ionization energies, *J. Mol. Model.*, 2010, **16**, 1679–1691.

90 J. S. Murray and P. Politzer, The electrostatic potential: an overview, *Wiley Interdiscip. Rev.: Comput. Mol. Sci.*, 2011, **1**, 153–163.

91 T. Clark,  $\sigma$ -Holes, *Wiley Interdiscip. Rev.: Comput. Mol. Sci.*, 2013, **3**, 13–20.

92 K. J. Donald, N. Pham and P. Ravichandran, Sigma Hole Potentials as Tools: Quantifying and Partitioning Substituent Effects, *J. Phys. Chem. A*, 2023, **127**, 10147–10158.

93 J. Halldin Stenlid and F. Abild-Pedersen, Revealing Local and Directional Aspects of Catalytic Active Sites by the Nuclear and Surface Electrostatic Potential, *J. Phys. Chem. C*, 2024, **128**, 4544–4558.

94 A. Michalak, M. Mitoraj and T. Ziegler, Bond orbitals from chemical valence theory, *J. Phys. Chem. A*, 2008, **112**, 1933–1939.

95 M. P. Mitoraj, A. Michalak and T. Ziegler, A combined charge and energy decomposition scheme for bond analysis, *J. Chem. Theory Comput.*, 2009, **5**, 962–975.

96 R. F. Nalewajski, J. Mrozek and A. Michalak, Two-electron valence indices from the Kohn-Sham orbitals, *Int. J. Quantum Chem.*, 1997, **61**, 589–601.

97 A. Michalak, R. L. DeKock and T. Ziegler, Bond multiplicity in transition-metal complexes: applications of two-electron valence indices, *J. Phys. Chem. A*, 2008, **112**, 7256–7263.

98 *The Chemical Bond: Fundamental Aspects of Chemical Bonding*, ed. G. Frenking and S. Shaik, Wiley-VCH Verlag GmbH & Co. KGaA, Weinheim, Germany, 2014.

99 X. Wang, Z. Wu, Z. Gong, D. Muhammad, B. Hu, P. Su and Z. Sun, All-atom Picture of Cucurbituril Detoxification Coordination, *ChemRxiv*, 2025, preprint, DOI: [10.26434/chemrxiv-2025-1x058-v2](https://doi.org/10.26434/chemrxiv-2025-1x058-v2).

100 T. Lu and Q. Chen, Independent gradient model based on Hirshfeld partition: A new method for visual study of interactions in chemical systems, *J. Comput. Chem.*, 2022, **43**, 539–555.

101 T. Lu and Q. Chen, *Comprehensive Computational Chemistry*, Elsevier, 2024, pp. 240–264.

102 C. Lefebvre, G. Rubez, H. Khartabil, J.-C. Boisson, J. Contreras-García and E. Hénon, Accurately extracting the signature of intermolecular interactions present in the NCI plot of the reduced density gradient versus electron density, *Phys. Chem. Chem. Phys.*, 2017, **19**, 17928–17936.

103 J. Contreras-García, E. R. Johnson, S. Keinan, R. Chaudret, J.-P. P. Piquemal, D. N. Beratan and W. Yang, NCIPLLOT: A Program for Plotting Noncovalent Interaction Regions, *J. Chem. Theory Comput.*, 2011, **7**, 625–632.

104 T. Lu and F. Chen, Multiwfn: a multifunctional wavefunction analyzer, *J. Comput. Chem.*, 2012, **33**, 580–592.

105 P. Procacci, Dealing with Induced Fit, Conformational Selection, and Secondary Poses in Molecular Dynamics Simulations for Reliable Free Energy Predictions, *J. Chem. Theory Comput.*, 2023, **19**, 8942–8954.

106 Z. Sun, Z. Huai, Q. He and Z. Liu, A General Picture of Cucurbit[8]uril Host–Guest Binding, *J. Chem. Inf. Model.*, 2021, **61**, 6107–6134.

107 X. Wang, S. Li, Z. Zhang, L. Qiu and Z. Sun, Multiscale Endpoint Screening with Extended Tight-binding Hamiltonians, *BIO Integr.*, 2025, **6**, e982.

108 L. Ueberricke, J. Schwarz, F. Ghalami, M. Matthiesen, F. Rominger, S. M. Elbert, J. Zaumseil, M. Elstner and M. Mastalerz, Triptycene End-Capped Benzothienobenzothiophene and Naphthothienobenzothiophene, *Chem. – Eur. J.*, 2020, **26**, 12596–12605.

109 G. R. Hutchison, M. A. Ratner and T. J. Marks, Hopping Transport in Conductive Heterocyclic Oligomers: Reorganization Energies and Substituent Effects, *J. Am. Chem. Soc.*, 2005, **127**, 2339–2350.

110 A. Das, N. Kamatham, A. Mohan Raj, P. Sen and V. Ramamurthy, Marcus Relationship Maintained During Ultrafast Electron Transfer Across a Supramolecular Capsular Wall, *J. Phys. Chem. A*, 2020, **124**, 5297–5305.

111 S. Mallick, L. Cao, X. Chen, J. Zhou, Y. Qin, G. Y. Wang, Y. Y. Wu, M. Meng, G. Y. Zhu, Y. N. Tan, T. Cheng and C. Y. Liu, Mediation of Electron Transfer by Quadrupolar Interactions: The Constitutional, Electronic, and Energetic Complementarities in Supramolecular Chemistry, *iScience*, 2019, **22**, 269–287.